REPORT DOCUMENTATION PAGE		Form Approved OMB No. 0704-0188

Public reporting burden for this collection of information is estimated to average 1 hour per response, including the time for reviewing instructions, searching existing data sources, gathering and maintaining the data needed, and completing and reviewing the collection of information. Send comments regarding this burden estimate or any other aspect of this collection of information, including suggestions for reducing this burden, to Washington Headquarters Services, Directorate for Information Operations and Reports, 1215 Jefferson Davis Highway, Suite 1204, Arlington, VA 22202-4302, and to the Office of Management and Budget, Paperwork Reduction Project (0704-0188), Washington, DC 20503.

1. AGENCY USE ONLY (Leave blank)	2. REPORT DATE 14.Mar.06	3. REPORT TYPE AND DATES COVERED MAJOR REPORT

4. TITLE AND SUBTITLE	5. FUNDING NUMBERS
A SEMICLASSICAL TRANSPORT MODEL FOR THIN QUANTUM BARRIERS.	

6. AUTHOR(S)
MAJ NOVAK KYLE A

7. PERFORMING ORGANIZATION NAME(S) AND ADDRESS(ES) UNIVERSITY OF WISCONSIN MADISON	8. PERFORMING ORGANIZATION REPORT NUMBER CI04-1749

9. SPONSORING/MONITORING AGENCY NAME(S) AND ADDRESS(ES) THE DEPARTMENT OF THE AIR FORCE AFIT/CIA, BLDG 125 2950 P STREET WPAFB OH 45433	10. SPONSORING/MONITORING AGENCY REPORT NUMBER

11. SUPPLEMENTARY NOTES

12a. DISTRIBUTION AVAILABILITY STATEMENT Unlimited distribution In Accordance With AFI 35-205/AFIT Sup 1	12b. DISTRIBUTION CODE

DISTRIBUTION STATEMENT A
Approved for Public Release
Distribution Unlimited

13. ABSTRACT (Maximum 200 words)

14. SUBJECT TERMS			15. NUMBER OF PAGES 23
			16. PRICE CODE

17. SECURITY CLASSIFICATION OF REPORT	18. SECURITY CLASSIFICATION OF THIS PAGE	19. SECURITY CLASSIFICATION OF ABSTRACT	20. LIMITATION OF ABSTRACT

A SEMICLASSICAL TRANSPORT MODEL
FOR THIN QUANTUM BARRIERS

SHI JIN AND KYLE A. NOVAK *

Abstract. We present a one-dimensional time-dependent semiclassical transport model for mixed state scattering with thin quantum barriers. The idea is to solve a stationary Schrödinger equation in the thin quantum barrier to obtain the scattering coefficients, and then use them to supply the interface condition that connects the two classical domains. We then build in the interface condition to the numerical flux, in the spirit of the Hamiltonian-preserving scheme introduced by Jin and Wen for a classical barrier. The overall cost is roughly the same as solving a classical barrier. We construct a numerical method based on this semiclassical approach and validate the model using various numerical examples.

Key words. multiscale method, semiclassical limit, Liouville, von Neumann, quantum barrier

AMS subject classifications. 65M06, 65Z05, 81Q20, 81S30, 81T80

1. Introduction. Advances in nanoscale materials fabrication technology have prompted the need for efficient numerical simulation of quantum structures. However, simulation is difficult when the system reacts over different length and time scales since the smaller scale usually drives the accuracy and consistency of the solution. Even when only interested in the macroscopic behavior, one may be forced to resolve the microscopic dynamics. Correspondence principles allow us to extract macroscopic behavior from microscopic dynamics in terms of a weak limit. When the scales act over several orders of magnitude, the numerical solution to the problem at the smallest scale becomes computationally intractable. In these cases, one often relies on a multiscale approach to provide a numerically efficient solution.

An example is the modeling of electron transport in nanostructures, such as resonant tunneling diodes, superlattices or quantum dots, where quantum phenomena in localized regions of the devices cannot be ignored. While one can use quantum mechanics in the entire region, it is clearly more computationally efficient to take a multiscale approach using classical mechanics in the rest of the device via a domain decomposition technique. Such a model was introduced by Ben Abdallah, Gamba and Degond, in which the interface conditions connecting the classical and the quantum regions were introduced to couple two classical regions with a quantum region [6, 7, 8].

This work is an extension of the Hamiltonian-preserving finite-volume method introduced by Jin and Wen [17, 16] for solving the multi-dimensional classical Liouville equation with a discontinuous (but classical) potential. The idea there was to build the interface condition, such as used in [7], that properly incorporates partial transmission and reflection information at the barrier into the numerical flux. This produces a scheme that connects momenta (velocities) on both sides of the barrier via the Hamiltonian preservation principle. Such a method is stable in both l^1 and l^∞ norms under a hyperbolic stability condition and captures sharply the weak semiclassical limit of the linear Schrödinger equation or geometrical optics through the barrier or interface.

*Department of Mathematics, University of Wisconsin, 480 Lincoln Drive, Madison, Wisconsin 53706-1338, USA (jin@math.wisc.edu, novak@math.wisc.edu) The views expressed in this article are those of the author and do not reflect the official policy or position of the United States Air Force, Department of Defense, or the U.S. Government.

The quantum barrier that separates the two classical regions differs from a classical barrier in that a quantum wave can tunnel through a barrier, be partially transmitted and reflected by a barrier, and resonate inside a barrier. Our idea is to solve the Schrödinger equation (either exactly if possible, or numerically via a transfer matrix method [1, 18, 12]) inside the quantum barrier in order to generate the transmission and reflection coefficients, and then use that information in the interface condition to solve the classical Liouville equation through the barrier, in the spirit of the Hamiltonian-preserving method of Jin and Wen. When the quantum barrier is thin (on the order of a de Broglie wavelength), solving the stationary Schrödinger equation suffices. Thus, our first step is merely preprocessing. Once the transmission and reflection coefficients are generated, the time marching is based on classical mechanics. Hence, our approach, which efficiently handles a thin quantum barrier, has a computational cost similar to a classical simulation in the entire device.

In §2 we review the correspondence between the classical and quantum mechanics. We then describe the quantum scattering at barriers in §3. We propose the semiclassical model and its numerical discretization §4. In §5 we present four numerical examples to verify and validate the semiclassical model the numerical method. Our numerical results indicate that the model captures correctly the solution of the Schrödinger equation in the entire domain in the limit of vanishing Planck constant.

2. Correspondence between classical and quantum mechanics.

2.1. From classical to quantum mechanics. A typical problem under consideration is particle flow through a solid-state device. If the potential is sufficiently smooth we may describe non-interacting particle dynamics in phase space classically as a Hamiltonian system

$$(2.1) \qquad \frac{dx}{dt} = \frac{p}{m} = \nabla_p H(x,p), \quad \frac{dp}{dt} = -\nabla_x V = -\nabla_x H(x,p)$$

where $x(t) \in \mathbb{R}^d$ is the particle position, $p(t) \in \mathbb{R}^d$ is the momentum, m is the effective mass and $V(x)$ is a time-independent potential. The Hamiltonian function $H(x,p)$ represents the total energy of the system

$$(2.2) \qquad H(x,p) = \frac{|p|^2}{2m} + V(x) = E.$$

One may introduce a probability distribution of particles $f(x,p,t)$ in phase space. By requiring that the probability be conserved along the particle trajectories one has

$$\frac{d}{dt}f = \frac{\partial}{\partial t}f + \frac{dx}{dt} \cdot \nabla_x f + \frac{dp}{dt} \cdot \nabla_p f = 0$$

and with the help of equation (2.1), one gets the classical Liouville equation

$$(2.3) \qquad \frac{\partial}{\partial t}f = \{H, f\} = \nabla_p f \cdot \nabla_x H - \nabla_x f \cdot \nabla_p H$$

where $\{\,\cdot\,,\,\cdot\,\}$ is the Poisson bracket. Alternatively,

$$(2.4) \qquad \frac{\partial}{\partial t}f + p \cdot \nabla_x f - \nabla_x V(x) \cdot \nabla_p f = 0.$$

By considering the zeroth-order moment of $f(x,p,t)$, one obtains the probability position density in physical space

$$\rho(x,t) = \int_{\mathbb{R}^d} f(x,p,t)\, dp,$$

2

which serves as a primary observable for the comparison of the model.

When the potential fluctuates rapidly over a short distance or the particles impinge on a sharp jump in potential, the classical description fails to capture the quantum wave-like nature of the particle and the Liouville description produces an incorrect solution. In particular, the classical Liouville equation does not model barrier tunneling, probabilistic partial reflection and transmission, or resonance which are crucial to the behavior of many modern electronic devices.

By considering Dirac quantization, one has the formal correspondence between the classical quantities and the quantum operators

$$\text{(2.5)} \qquad x \;\to\; x, \qquad p \;\to\; -i\hbar\nabla, \qquad \text{and} \qquad E \;\to\; i\hbar\tfrac{\partial}{\partial t},$$

where $\hbar$ is Planck's constant. Using this quantization, one obtains the Schrödinger equation from the classical Hamiltonian (2.2)

$$\text{(2.6)} \qquad i\hbar\frac{\partial}{\partial t}\psi = \hat{H}\psi = \left(-\frac{\hbar^2}{2m}\Delta + V(x)\right)\psi$$

which describes the time evolution of the probability amplitude $\psi(x,t;\tilde{x},\tilde{p})$ initially centered at $\tilde{x}$ with an initial energy state $E = H(\tilde{x},\tilde{p})$. The square of the magnitude of the probability amplitude $\rho(x,t) = |\psi(x,t)|^2$ gives the position density in physical space.

Instead of considering a pure state system, one may also consider a mixed state system for which the initial state $H(x,p)$ of the particle is given in terms of a macroscopic statistical distribution $\tilde{f}(x,p)$. Define the density matrix as

$$\text{(2.7)} \qquad \hat{\rho}(x,x',t) = \int_{\mathbb{R}^d}\int_{\mathbb{R}^d} \tilde{f}(\tilde{x},\tilde{p})\psi(x,t;\tilde{x},\tilde{p})\overline{\psi}(x',t;\tilde{x},\tilde{p})\,d\tilde{x}\,d\tilde{p}.$$

The time evolution of the density matrix is found by taking the partial derivative of equation (2.7) with respect to t. By using the Schrödinger equation (2.6) and the hermicity of Hamiltonian operator $\hat{H}$, one obtains the von Neumann equation

$$\text{(2.8)} \qquad i\hbar\frac{\partial}{\partial t}\hat{\rho}(x,x',t) = \left(-\frac{\hbar^2}{2m}[\Delta_x - \Delta_{x'}] + V(x) - V(x')\right)\hat{\rho}(x,x',t).$$

The von Neumann representation may be thought of as the fundamental description of quantum mechanics [9]. By taking $\tilde{f}(\tilde{x},\tilde{p}) = \delta(\tilde{x}-x_0)\delta(\tilde{p}-p_0)$ in (2.7), the density matrix reduces to $\hat{\rho}(x,x',t) = \psi(x,t;x_0,p_0)\overline{\psi}(x',t;x_0,p_0)$ and the physical observables of the mixed state von Neumann equation correspond to those of the pure state Schrödinger equation. In this manner, the Schrödinger equation is simply a limiting case of the von Neumann equation. By taking the diagonal of the density matrix, one gets the position density in physical space

$$\hat{\rho}(x,x,t) = \int_{\mathbb{R}^d}\int_{\mathbb{R}^d} \tilde{f}(\tilde{x},\tilde{p})|\psi(x,t;\tilde{x},\tilde{p})|^2\,d\tilde{x}\,d\tilde{p}.$$

2.2. Semiclassical limit: quantum to classical. Consider a characteristic length and time scale $L\delta x$ and $L\delta t$ where δx is the natural length scale such as a de Broglie wavelength $\delta x = \hbar/p$ for some momentum p. By rescaling x,x' and t

$$x \mapsto x/L\delta x, \quad x' \mapsto x'/L\delta x, \quad t \mapsto t/L\delta t$$

3

in the von Neumann equation we have

$$(2.9) \qquad i\varepsilon\frac{\partial}{\partial t}\hat{\rho}(x,x',t) = \left(-\frac{\varepsilon^2}{2m}[\Delta_x - \Delta_{x'}] + V(x) - V(x')\right)\hat{\rho}(x,x')$$

where the dimensionless scaled Planck constant $\varepsilon = [mL(\delta x)^2/\delta t]^{-1}\hbar$ and the effective mass m has been nondimensionalized. Solving the Schrödinger and von Neumann equations numerically presents several difficulties. The de Broglie wavelength must be resolved numerically to ensure correct physical observables of the solution. Typically, this requires that the mesh size $\Delta x = O(\varepsilon)$ or even $o(\varepsilon)$ with a similar constraint on the time discretization Δt [4, 24]. When ε is small, computation is expensive since we need to use $O(N^{d+1})$ operations to compute the Schrödinger solution and $O(N^{2d+1})$ operations to compute the von Neumann solution where $N = O(\varepsilon^{-1})$ is the number of grid points in each space dimension. Because of such reasons, semiclassical methods are important for the solutions when $\varepsilon \ll 1$.

A typical path to the derivation of semiclassical limit is through the WKB approximation. However, the WKB approximation to the Schrödinger equation fails to capture multiphase information beyond caustics [14, 29]. An alternative method is to use the Wigner transform, the Fourier transform of the density matrix,

$$(2.10) \qquad W(x,p,t) = \frac{1}{(2\pi)^d}\int_{\mathbb{R}^d}\hat{\rho}(x + \tfrac{1}{2}\varepsilon y, x - \tfrac{1}{2}\varepsilon y, t)e^{-ip\cdot y}\,dy.$$

By applying the transform to the von Neumann equation one has the Wigner equation [31]

$$\frac{\partial}{\partial t}W + \frac{p}{m}\cdot\nabla_x W - \Theta^\varepsilon W = 0$$

where the nonlocal term

$$\Theta^\varepsilon W(x,p,t) = \frac{1}{(2\pi)^d}\int_{\mathbb{R}^d}\frac{i}{\varepsilon}\left[V(x + \tfrac{1}{2}\varepsilon y) - V(x - \tfrac{1}{2}\varepsilon y)\right]\check{W}(x,y,t)e^{-ip\cdot y}\,dy.$$

with

$$\check{W}(x,y,t) = \int_{\mathbb{R}^d}W(x,p,t)e^{ip\cdot y}\,dp$$

being the inverse Fourier transform of $W(x,p,t)$. When the potential $V(x)$ is sufficiently smooth, one recovers the classical Liouville equation in the limit as $\varepsilon \to 0$ [10, 22]

$$(2.11) \qquad \frac{\partial f}{\partial t} + \frac{p}{m}\cdot\nabla_x f - \nabla_x V\cdot\nabla_p f = 0.$$

However, the classical limit is not valid at the discontinuties of the potential [3, 27, 28], where the potential behaves as a quantum scatterer. In the case of a quantum barrier, we may consider a multiscale domain decomposition approach for a solution [7]. In the next section, we present a semiclassical model of a thin quantum barrier with the mixed-state dynamics.

4

3. Particle behavior at a quantum barrier. To model quantum dynamics, we consider a top-down multiscale approach by considering the quantum effects as local corrections to the global classical particle dynamics. In order to isolate and simplify the problem, we make the following assumptions/limitations:

1. The dynamics are restricted to one dimension.

2. The effective width of a barrier is $O(\varepsilon)$. On the classical scale, this means that we may approximate it as having zero width; on the quantum scale, this means that we may typify it as a single scattering center and we may neglect particle dwell time in the quantum region in the semiclassical limit.

3. The distance between neighboring barriers is $O(1)$ and hence each barrier may be considered independently.

4. The change in the potential $\nabla_x V(x)$ is $O(1)$ except at quantum barriers.

5. The coherence time is sufficiently short and therefore we may neglect interference away from the barrier.

Naturally, one would like to be able to treat a wider class of problems including periodic crystalline domains and mesoscopic barriers for which ε is nonvanishing. We will examine corrections and extensions to these simplifications in subsequent papers.

We begin with the Hamiltonian system discussed in §2

$$\frac{d}{dt}x = \nabla_p H(x,p), \quad \frac{d}{dt}p = -\nabla_x H(x,p).$$

Let a *bicharacteristic* of the function $H(x,p)$ be the integral curve $\varphi(t) = (x(t), p(t))$. Note that $\varphi(t)$ may not be defined for all time $t \in \mathbb{R}$. When $H(\varphi(t))$ is differentiable,

$$(3.1) \qquad \frac{d}{dt}H(\varphi(t)) = \frac{d}{dt}x \cdot \nabla_x H + \frac{d}{dt}p \cdot \nabla_p H = 0$$

from which it follows that the Hamiltonian is constant along any bicharacteristic $\varphi(t)$, *i.e.*,

$$(3.2) \qquad H(\varphi(t)) = \text{const.}$$

Condition (3.1) may be interpreted as the strong form of the conservation of energy, while condition (3.2) may be interpreted as the weak form. If the potential $V(x)$ is discontinuous or not defined in some region $Q \in \mathbb{R}^d$, the Liouville equation fails to have a global solution since $\nabla_x V(Q)$ is undefined.

The key idea behind Hamiltonian preserving schemes [17, 16] is to (a) solve the Liouville equation locally; (b) use the weak form of the conservation of energy to connect the local solutions together; and (c) incorporate a physically relevant interface condition to choose the correct solution. Let $\mathcal{L}$ be the locally defined set of bicharacteristics of the function $H(x,p)$. By requiring the Hamiltonian to be constant along trajectories, we create an equivalence class of bicharacteristics $[\varphi] = \{ \varphi^* \in \mathcal{L} \mid H(\varphi^*) = H(\varphi) \}$.

Generating a *global bicharacteristic* is a matter of connecting equivalent bicharacteristics at the barriers. If we consider the incident and scattered trajectory limits $(x(t^-), p(t^-))$ and $(x(t^+), p(t^+))$ on a barrier in one-dimensional phase space, then from equation (2.2) the scattered momenta are

$$(3.3a) \qquad p(t^+) = -p(t^-)$$

for reflection and

$$(3.3b) \qquad p(t^+) = \text{sign}[p(t^-)]\sqrt{|p(t^-)|^2 + 2m[V(x(t^-) - V(x(t^+))]}$$

5

for transmission. Unless $|p(t^-)|^2 < 2m[V(x(t^+)) - V(x(t^-))]$, for which the transmitted momentum is imaginary, the conservation of energy does not tell us which of these two bicharacteristics a particle should physically follow. In order to resolve the nonuniqueness, we require an additional interface condition which we derive from the Schrödinger solution across the interface. By interpreting a wave function as a statistical ensemble of a large number of particles [26], we have the interface condition

$$(3.4) \qquad f(x(t^+), p(t^+)) = R(p_r(t^-))f(x(t^+), p_r(t^-)) + T(p_t(t^-))f(x(t^-), p_t(t^-))$$

where $T(p)$ denotes the probability of an incident particle being transmitted across some region, $R(p)$ denotes the probability of an incident particle being reflected, and the incident momenta

$$p_r(t^-) = -p(t^+) \quad \text{and}$$
$$p_t(t^-) = \text{sign}[p(t^+)]\sqrt{|p(t^+)|^2 + 2m[V(x(t^+) - V(x(t^-))]}$$

come from equations (3.3b) and (3.3a).

We assume that the probability of a particle being absorbed by the barrier is zero and hence $T(p) + R(p) = 1$. By defining

$$T(p(t^-)) = \begin{cases} 1 & \text{if } |p(t^-)|^2 > 2m\left[V(x(t^+)) - V(x(t^-))\right] \text{ and} \\ 0 & \text{otherwise}, \end{cases}$$

i.e., total transmission/reflection, condition (3.4) reduces the classical Liouville solution for which bicharacteristics are uniquely determined for each (x, p). When $T(p) \in (0, 1)$, i.e., partial transmission/reflection, the bicharacteristics are no longer unique and instead we consider multiple bicharacteristic solutions.

Every interaction with a barrier potentially introduces a reflected and transmitted solution resulting in an additional bicharacteristic. We may enumerate the solutions and define a *bicharacteristic solution* to the Liouville equation as

$$f_k(x, p, t) = \int \tilde{f}(\tilde{x}, \tilde{p})\varphi_k(x, p, t; \tilde{x}, \tilde{p}) \, d\tilde{x} \, d\tilde{p}$$

where

$$\varphi_k(x, p, t; \tilde{x}, \tilde{p}) = \delta(x(t) - \tilde{x})\delta(p(t) - \tilde{p})$$

is the kth global bicharacteristic for $H(\tilde{x}, \tilde{p})$. By linearity of the Liouville equation we may consider the general solution as the superposition of the bicharacteristic solutions

$$(3.5) \qquad f(x, p, t) = \sum_k c_k(H(x, p))f_k(x, p, t).$$

where $c_k(H(x, p))$ is product of reflection and transmission probabilities along the kth bicharacteristic.

Except for simple solutions such as the global-in-time solution for a piecewise-constant potential or the local-in-time solution for a piecewise-quadratic potential, an exact solution cannot be explicitly given. Even for a simple discontinuous oscillator the number of bicharacteristics that need to be tracked becomes cumbersome in a short time interval. See Fig. 3.1. By solving the model numerically, we mitigate these difficulties.
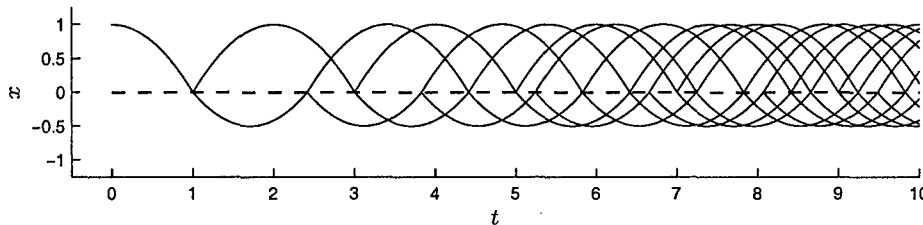
FIG. 3.1. *Particle position as a function of time for potential $V(x) = 2|x| - H(x)$ where $H(x)$ is the Heaviside step function. Particle has initial conditions $\delta(x+1)\delta(p)$.*

4. A semiclassical approach and numerical discretization.

4.1. A semiclassical approach.
When the quantum barrier is sufficiently narrow, the barrier may be modeled using the time-independent Schrödinger equation. We may then derive the transmission/reflection probabilities for the interface condition (3.4) by considering the current density. The interface condition is used to connect two classical domains modeled by the classical Liouville equation (2.11).

We consider an algorithm consisting of an initialization routine and a Liouville solver:

    1. During initialization, we determine the stationary states at the barrier by solving the time-independent Schrödinger equation. The solutions may be found by considering the barrier as an open quantum system [2] outside of which the potential is constant. Typically, this may be done by using a quantum transmitting boundary method [20], a spectral projection method [23], or a transfer matrix method [1, 18, 12]. With this solution, we compute the scattering information, namely the transmission and reflection coefficients.

    2. Following initialization, we solve the Liouville equation using a finite volume method. As done in [15] the interface condition (3.4) is built into the numerical flux in a framework called the Hamilton preserving scheme. This yields a numerical scheme for which the stability condition—the CFL condition—is hyperbolic, namely $\Delta t = O(\Delta x, \Delta p)$ with l^∞ and l^1 stability. See [15].

This approach aims at capturing the weak limit of the Schrödinger and von Neumann equations as $\varepsilon \to 0$, without solving the Schrödinger or von Neumann equations over the entire domain, but rather just at the quantum barrier and only in the initialization step. We now discuss the initialization routine and the finite volume routine in detail.

4.2. Routine initialization.
We use the transfer matrix method because it is robust over a wide range of momenta. On the quantum scale we decompose a one-dimensional barrier into a sequence of step potentials over which we solve the time-independent Schrödinger equation exactly. Take a quantum barrier in the bounded region $Q = [x_1, x_2]$ and take the potential to be constant outside this barrier—$V(x) = V_1$ in $C_1 = (-\infty, x_1)$ and $V(x) = V_2$ in $C_1 = (x_2, \infty)$. For a state $E = p^2/2m$ the time-independent Schrödinger equation
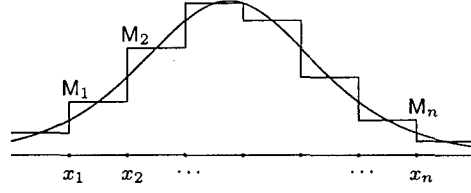
$$-\varepsilon\psi''(x) + 2mV(x)\psi(x) = p^2\psi(x)$$

7

FIG. 4.1. *Approximation of a potential barrier by a series of step potentials. The effective transfer matrix* $\mathsf{M} = \mathsf{M}_n \cdots \mathsf{M}_2 \mathsf{M}_1$ *where* M_j *is the transfer matrix for a step potential at* x_j.

has the solution

$$(4.1) \qquad \psi(x) = \begin{cases} a_1 e^{i\kappa_1(x-x_1)/\varepsilon} + b_1 e^{-i\kappa_1(x-x_1)/\varepsilon}, & x \in \mathcal{C}_1, \\ \psi_{\mathcal{Q}}, & x \in \mathcal{Q} \\ a_2 e^{i\kappa_2(x-x_2)/\varepsilon} + b_2 e^{-i\kappa_2(x-x_2)/\varepsilon}, & x \in \mathcal{C}_2 \end{cases}$$

where $\kappa_{1,2} = \sqrt{p^2 - 2mV_{1,2}}$ and the coefficients a_1, a_2, b_1 and b_2 are uniquely determined by the boundary conditions at x_1 and x_2. By requiring that the solution $\psi(x)$ and its derivative be continuous, $\psi_{\mathcal{Q}}$ is uniquely determined by the values a_1 and b_1 using the boundary conditions $\psi_{\mathcal{Q}}(x_1)$ and $\psi'_{\mathcal{Q}}(x_1)$. In turn, the values a_2 and b_2 are uniquely determined by the values $\psi_{\mathcal{Q}}(x_2)$ and $\psi'_{\mathcal{Q}}(x_2)$. Since the Schrödinger equation is linear, a_2 and b_2 may be expressed as linear functions of a_1 and b_1. Hence, for each momentum p we may relate the solution in $\mathcal{C}_2$ with the solution $\mathcal{C}_1$ in terms of the transfer matrix M

$$(4.2) \qquad \begin{pmatrix} a_2 \\ b_2 \end{pmatrix} = \mathsf{M} \begin{pmatrix} a_1 \\ b_1 \end{pmatrix} = \begin{pmatrix} m_{11} & m_{12} \\ m_{21} & m_{22} \end{pmatrix} \begin{pmatrix} a_1 \\ b_1 \end{pmatrix}.$$

An arbitrary quantum barrier may be discretized and approximated by a series of step potentials, for each of which a transfer matrix may be computed analytically. Specifically, the transfer matrix may be approximated as $\mathsf{M} = \mathsf{M}_n \cdots \mathsf{M}_2 \mathsf{M}_1$ with $\mathsf{M}_j = \mathsf{D}_{j+1}^{1/2} \mathsf{P}_j \mathsf{D}_j^{1/2}$ where

$$(4.3) \qquad \mathsf{P}_j = \tfrac{1}{2} \begin{pmatrix} 1 + \kappa_j/\kappa_{j+1} & 1 - \kappa_j/\kappa_{j+1} \\ 1 - \kappa_j/\kappa_{j+1} & 1 + \kappa_j/\kappa_{j+1} \end{pmatrix}$$

is the transfer matrix associated with a potential jump $V(x_j^+) - V(x_j^-)$ and

$$(4.4) \qquad \mathsf{D}_j = \begin{pmatrix} \exp(i\Delta x \kappa_j/\varepsilon) & 0 \\ 0 & \exp(-i\Delta x \kappa_j/\varepsilon) \end{pmatrix}.$$

is the transfer matrix associated with the displacement $\Delta x = x_j - x_{j-1}$.

One may also express the solutions in $\mathcal{C}_1$ and $\mathcal{C}_2$ in terms of a scattering matrix S which relates the incident and scattered waves

$$(4.5) \qquad \begin{pmatrix} b_1 \\ a_2 \end{pmatrix} = \mathsf{S} \begin{pmatrix} a_1 \\ b_2 \end{pmatrix} = \begin{pmatrix} r_1 & t_2 \\ t_1 & r_2 \end{pmatrix} \begin{pmatrix} a_1 \\ b_2 \end{pmatrix} = \begin{pmatrix} -m_{21}/m_{22} & 1/m_{22} \\ \Delta/m_{22} & m_{12}/m_{22} \end{pmatrix} \begin{pmatrix} a_1 \\ b_2 \end{pmatrix}.$$

where $\Delta = \det \mathsf{M} = m_{22}m_{11} - m_{12}m_{21}$. By considering the time evolution of the position density $\rho(x,t) = |\psi(x,t)|^2$ in the Schrödinger equation, one derives the continuity equation

$$\frac{\partial}{\partial t}\rho + \nabla \cdot J = 0$$

where the current-density is defined as $J(x) = \varepsilon m^{-1} \mathrm{Im}\left(\overline{\psi}\nabla\psi\right)$. From equations (4.1), one has that

$$(4.6) \qquad J(x) = \begin{cases} \kappa_1 \left(|a_1|^2 - |b_1|^2\right)/m, & x \in \mathcal{C}_1 \\ \kappa_2 \left(|a_2|^2 - |b_2|^2\right)/m, & x \in \mathcal{C}_2 \end{cases}$$

where m is the effective particle mass. The positive-valued terms of the $J(x)$ express the flux of right-traveling waves and the negative-valued terms express the flux of left-traveling waves. In particular, for a wave incident on the barrier from the left $(b_2 \equiv 0)$, we have $a_2 = t_1 a_1$ and $b_1 = r_1 a_1$. It follows that the reflection coefficient R_1, the ratio of the reflected to incident current densities, and the transmission coefficient T_1, the ratio of the transmitted to incident current densities, are

$$(4.7) \qquad R_1 = |r_1|^2 \qquad \text{and} \qquad T_1 = (\kappa_2/\kappa_1)|t_1|^2.$$

Similarly, for a wave incident from the right

$$(4.8) \qquad R_2 = |r_2|^2 \qquad \text{and} \qquad T_2 = (\kappa_1/\kappa_2)|t_2|^2.$$

The transmission and reflection coefficients are uniquely determined along a bicharacteristic. It is clear by time-reversibility that the transmission coefficient along any bicharacteristic is independent of direction

$$(4.9) \qquad T_1(p) = T_2\left(-\sqrt{p^2 + 2m(V_2 - V_1)}\right).$$

4.3. A Liouville solver. Without loss of generality, we shall take the mass $m = 1$ in which case we equate the velocity with the momentum p. To solve the semiclassical Liouville equation (2.11), we use a Hamiltonian-preserving finite-volume method [17]. We consider a uniform mesh in phase space with grid points at $(x_{i+1/2}, p_{j+1/2})$ and denote grid spacing $\Delta x = x_{i+1/2} - x_{i-1/2}$ and $\Delta p = p_{j+1/2} - p_{j-1/2}$ with $i, j \in \mathbb{Z}$. Let the cell centers be $x_i = \frac{1}{2}(x_{i+1/2} + x_{i-1/2})$ and $p_j = \frac{1}{2}(p_{j+1/2} + p_{j-1/2})$. For convenience of notation, we shall take $p_0 \equiv 0$ and $p_{-j} = -p_j$. We shall consider the quantum barrier to be located at a cell interface $x_{Z+1/2}$ for some integer(s) Z.

Define the cell average over the cell $C_{ij} = [x_{i-1/2}, x_{i+1/2}] \times [p_{j-1/2}, p_{j+1/2}]$ as

$$f_{ij}^n = \frac{1}{\Delta x \Delta p} \iint_{C_{ij}} f(x, p, t_n)\, dx\, dp.$$

The finite-volume discretization of the one-dimensional Liouville equation (2.11) is

$$(4.10) \qquad f_{ij}^{n+1} = f_{ij}^n - \Delta t \left[p_j \partial_x f_{ij}^n - \partial_x V_i \partial_p f_{ij}^n\right].$$

where the discrete operators $\partial_x f_{ij}$, $\partial_p f_{ij}$ and $\partial_x V_i$ are

$$\partial_x f_{ij} = (f_{i+1/2,j}^- - f_{i-1/2,j}^+)/\Delta x,$$
$$\partial_p f_{ij} = (f_{i,j+1/2} - f_{i,j-1/2})/\Delta p, \text{ and}$$
$$\partial_x V_i = (V_{i+1/2}^- - V_{i-1/2}^+)/\Delta x$$

9

with

$$f^{\pm}_{i+1/2,j} = \lim_{x \to x^{\pm}_{i+1/2}} \frac{1}{\Delta p} \int_{p_{j-1/2}}^{p_{j+1/2}} f(x,p)\,dp,$$

$$f_{i,j+1/2} = \frac{1}{\Delta x} \int_{x_{i-1/2}}^{x_{i+1/2}} f(x,p_{j+1/2})\,dx, \text{ and}$$

$$V^{\pm}_{i+1/2} = \lim_{x \to x^{\pm}_{i+1/2}} V(x).$$

Upwinding is used to approximate the fluxes $f^{\pm}_{i+1/2,j}$ and $f_{i,j+1/2}$. If the potential $V(x)$ is continuous at some point $x_{i+1/2}$, then $p(t^+) = p(t^-)$ and hence $f^-_{i+1/2,j} = f^+_{i+1/2,j}$ which reduces the discretized Liouville equation (4.10) to the usual upwind finite volume scheme. At the barrier $x_{Z+1/2}$, special consideration must be taken.

From conservation of the Hamiltonian (3.3) we have that the incident velocity q_j (upwind of the barrier) for a particle transmitted with velocity p_j is

$$q_{\pm|j|} = \pm\sqrt{p^2_{\pm|j|} \pm 2(V^+_{Z+1/2} - V^-_{Z+1/2})}.$$

Similarly, the transmitted velocity (downwind of the barrier) for a particle incident with velocity p_j is $-q_{-j}$. The incident velocity for a particle reflected with velocity p_j is simply $-p_j$. Note that, whereas $-p_{-j} = p_j$, in general $-q_{-j} \neq q_j$. Further note that by time reversibility $T(q_{-j}) = T(p_j)$ and $R(q_{-j}) = R(p_j)$.

The left and right limits of the probability distribution f in the cells immediately downwind of the quantum barrier are determined by the interface condition (3.4)

$$f^+_{Z+1/2,j} = R(q_j)f^+_{Z+1/2,-j} + T(q_j)f(x^-_{Z+1/2},q_j) \qquad \text{for } j > 0$$

$$f^-_{Z+1/2,j} = R(q_j)f^-_{Z+1/2,-j} + T(q_j)f(x^+_{Z+1/2},q_j) \qquad \text{for } j < 0.$$

The values for $f(x^{\pm}_{Z+1/2},q_j)$ are approximated in a manner similar to Scheme II of [17]. Consider the flux incident from the left ($q_j > 0$)—the same treatment applies to flux incident from the right. We define $f(x^-_{Z+1/2},q_j)$ as the cell average

(4.11) $$f(x^-_{Z+1/2},q_j) = \frac{1}{p_j\Delta p} \int_{q_{j-1/2}}^{q_{j+1/2}} pf(x^-_{Z+1/2},p)\,dp$$

where

$$q_{j\pm1/2} = \sqrt{p^2_{j\pm1/2} + 2(V^+_{Z+1/2} - V^-_{Z+1/2})}.$$

The integral is approximated by a composite mid-point rule. Since the limits of the integral are not generally gridpoints in the p-direction, some care must be taken. If $p_{k-1/2} \le q_{j-1/2} < q_{j+1/2} \le p_{k+1/2}$ for some k, then we take

$$f(x^-_{Z+1/2},q_j) = f^-_{Z+1/2,k} + \overline{q}_j\sigma_p(f^-_{Z+1/2,k})$$

where the slope $\sigma_p(\cdot)$ in the p-direction is calculated using the Van Leer limiter

(4.12) $$\sigma_p(f_{ij}) = \left(\frac{f_{ij} - f_{i,j-1}}{\Delta p}\right)\phi\left(\frac{f_{i,j+1} - f_{ij}}{f_{ij} - f_{i,j-1}}\right)$$

10

with $\phi(\theta) = (\theta + |\theta|)/(1 + |\theta|)$ [21]. Otherwise $p_{k-1/2} \le q_{j-1/2} < \cdots < q_{j+1/2} \le p_{k+s+1/2}$ for some k and s, and we take

(4.13) $\quad f(x^-_{Z+1/2}, q_j) =$

$$\frac{1}{p_j \Delta p} \left\{ (p_{k+1/2} - q_{j-1/2}) \left[p_k f^-_{Z+1/2,k} + \tfrac{1}{2}(p_{k+1/2} + q_{j-1/2})\sigma_p(p_k f^-_{Z+1/2,k}) \right] + \right.$$

$$p_{k+1}\Delta p f^-_{Z+1/2,k+1} + \cdots + p_{k+s-1}\Delta p f^-_{Z+1/2,k+s-1} +$$

$$\left. (q_{j+1/2} - p_{k+s-1/2}) \left[p_{k+s} f^-_{Z+1/2,k+s} + \tfrac{1}{2}(p_{k+s-1/2} + q_{j+1/2})\sigma_p(p_{k+s} f^-_{Z+1/2,k+s}) \right] \right\}.$$

For a second-order accurate method we use a slope-limited piecewise-linear interpolant to approximate the right and left density limits

(4.14) $$f^\pm_{i\mp 1/2,j} = f_{ij} \mp \tfrac{1}{2}(1 - \lambda_j)\Delta x \sigma_x(f_{ij})$$

where $\lambda_j = |v_j|\Delta t/\Delta x$ and the slope $\sigma_x(\cdot)$ in the x-direction is calculated using the Van Leer limiter

(4.15) $$\sigma_x(f_{ij}) = \left(\frac{f_{ij} - f_{i-1,j}}{\Delta x} \right) \phi \left(\frac{f_{i+1,j} - f_{ij}}{f_{ij} - f_{i-1,j}} \right).$$

Since the slope $\sigma_x(\cdot)$ is a function of $f_{i-1,j}$, $f_{i,j}$ and $f_{i+1,j}$ and the density f is not necessarily continuous across the barrier in the x-direction, we can not directly use (4.14) and (4.15) to calculate the density limits at the barrier interface. Rather, we first need to construct the ghost densities f^*_Z and f^*_{Z+1} across the barrier using the scattered densities at x_Z and x_{Z+1} based on conservation of mass. Specifically, downwind of the barrier

$$f^+_{Z+1/2} \equiv f^+_{Z+1/2}(f^*_Z, f_{Z+1}, f_{Z+2}) \quad \text{and} \quad f^-_{Z+1/2} \equiv f^-_{Z+1/2}(f_{Z-1}, f_Z, f^*_{Z+1})$$

with ghost densities f^*_Z and f^*_{Z+1} located upwind of the barrier; and upwind of the barrier

$$f^+_{Z-1/2} \equiv f^+_{Z-1/2}(f_{Z-1}, f_Z, f^*_{Z+1}) \quad \text{and} \quad f^-_{Z+3/2} \equiv f^-_{Z+3/2}(f^*_Z, f_{Z+1}, f_{Z+2})$$

with ghost densities f^*_Z and f^*_{Z+1} located downwind of the barrier.

Construction of the ghost densities is analogous to using ghost cells to enforce semipermeable inflow and outflow reflecting boundary conditions. To calculate the ghost densities *upwind* of the barrier we use the interface condition (3.4) to mix together the densities upwind of the barrier that will subsequently be combined through transmission and reflection. In this case,

$$f^*_{Z,j} = R(q_j)f_{Z+1,-j} + T(q_j)f(x_Z, q_j) \qquad \text{for } j > 0,$$

$$f^*_{Z+1,j} = R(q_j)f_{Z,-j} + T(q_j)f(x_{Z+1}, q_j) \qquad \text{for } j < 0.$$

To calculate the ghost densities *downwind* of the barrier we unmix the densities downwind of the barrier that were previously combined through transmission and reflection at the barrier. In this case,

$$f^*_{Z+1,j} = \frac{T(p_j)f(x_{Z+1}, -q_{-j}) - R(p_j)f_{Z,-j}}{T(p_j) - R(p_j)} \qquad \text{for } j > 0,$$

$$f^*_{Z,j} = \frac{T(p_j)f(x_Z, -q_{-j}) - R(p_j)f_{Z+1,-j}}{T(p_j) - R(p_j)} \qquad \text{for } j < 0.$$

11

In both cases, the densities $f(x_{Z+1}, \pm q_{\pm j})$ and $f(x_Z, \pm q_{\pm j})$ are approximated in a manner similar to (4.11).

To approximate $f_{i,j+1/2}^{\pm}$ to second-order in the p-direction we have

$$f_{i,j\mp1/2}^{\pm} = f_{i,j} \mp \tfrac{1}{2}(1 - \lambda_i)\Delta p \sigma_p(f_{ij})$$

with $\lambda_i = |\partial_x V_i|\Delta t/\Delta p$ and the slope $\sigma_p(\cdot)$ defined using the van Leer limiter (4.12).

5. Numerical examples. In this section, we present a few examples of both pure state dynamics and mixed state dynamics in order to verify and validate the semiclassical model and numerical scheme.

For a mixed state solution with a macroscopic distribution, we are not limited by the support of the wavepacket and the complexity of the scheme is $O((\Delta x \Delta p \Delta t)^{-1})$ where Δx, Δp, and $\Delta t \gg \varepsilon$. For direct simulation of the von Neumann equation, not only must we resolve ε in space and time but we must solve the equation over two space dimensions and one time dimension so the complexity of the scheme is $O(\varepsilon^{-3})$. When $\varepsilon \ll 1$, the computing time for a direct von Neumann solution is considerably longer than for the multiscale semiclassical Liouville solution.

The numerical Schrödinger solution may be computed using the Crank-Nicolson operator

$$(5.1) \qquad \psi(x_i, t + \Delta t) = (1 + i\varepsilon^{-1}\Delta t H_D)^{-1}(1 - i\varepsilon^{-1}\Delta t H_D)\psi(x_i, t)$$

where the discrete Hamiltonian operator

$$(5.2) \qquad H_D = \frac{-\varepsilon^2}{2m}\frac{\delta_{i,i-1} - 2\delta_{ii} + \delta_{i,i+1}}{(\Delta x)^2} + V(x_i)$$

with Kronecker delta $\delta_{ii} = 1$ and $\delta_{ij} = 0$ if $i \neq j$. Markowich *et al.* [24] show that for such a scheme, in order to guarantee correct approximation to physical observables for small ε, one needs to take $\Delta x = o(\varepsilon)$ and $\Delta t = o(\varepsilon)$. One may also compute the numerical Schrödinger solution using a pseudospectral method with Strang splitting [4]. In this case, one splits the kinetic and potential terms, so that for each time step

$$\psi(x, t + \Delta t) = e^{\Delta t B/2} \mathcal{F}^{-1}\left[e^{\Delta t A} \mathcal{F}\left[e^{\Delta t B/2}\psi(x, t)\right]\right]$$

where

$$A = \frac{\varepsilon}{2mi}k^2 \qquad \text{and} \qquad B = \frac{1}{i\varepsilon}V(x)$$

and the operators $\mathcal{F}$ and $\mathcal{F}^{-1}$ denote the one-dimensional discrete Fourier transform and discrete inverse Fourier transform with respect to the x and k variables. One can use a mesh that is coarser than the mesh required by a finite-difference method to resolve ε and capture the correct dynamics [4, 5]. Based on numerical observation, we find that we require $\Delta x < \varepsilon/4$ to ensure numerical convergence to the correct physical observables and for numerical error to be insignificant. When the potential is discontinuous, we find that the solution exhibits artificial oscillations unless $\Delta t < (\Delta x)^2/\varepsilon$ and $\Delta t < \varepsilon/V(x)$.

The von Neumann equation

$$i\varepsilon\frac{\partial}{\partial t}\hat{\rho} = \hat{H}\hat{\rho} - (\hat{H}\hat{\rho}^T)^T \qquad \text{with} \qquad \hat{H} = -\frac{\varepsilon^2}{2m}\partial_{xx} + V(x)$$

has the formal solution

$$\hat{\rho}(x, x', t + \Delta t) = e^{i\varepsilon \Delta t \hat{H}} \hat{\rho}(x, x', t) e^{-i\varepsilon \Delta t \hat{H}}.$$

By using the discrete Hamiltonian operator (5.2), we may approximate the von Neumann solution in terms of the Crank-Nicolson operator (5.1) to get a method without splitting error

$$\hat{\rho}_{ij}^{n+1} = (1 + i\varepsilon^{-1}\Delta t H_D)^{-1}(1 - i\varepsilon^{-1}\Delta t H_D)\hat{\rho}_{ji}^{\star} \quad \text{with}$$

$$\hat{\rho}_{ij}^{\star} = (1 - i\varepsilon^{-1}\Delta t H_D)^{-1}(1 + i\varepsilon^{-1}\Delta t H_D)\hat{\rho}_{ji}^{n}$$

where $\rho_{ij}^n = \hat{\rho}(x_i, x_j', t_n)$. We may also solve the von Neumann equation using a pseudospectral method with Strang splitting [13],

$$\hat{\rho}^{n+1} = e^{\Delta t B/2} \mathcal{F}^{-1} \left(e^{\Delta t A} \mathcal{F} \left(e^{\Delta t B/2} \hat{\rho}^n \right) \right)$$

where

$$A = \frac{\varepsilon}{2mi}(k^2 - k'^2) \qquad \text{and} \qquad B = \frac{1}{i\varepsilon}(V(x) - V(x'))$$

and the operators $\mathcal{F}$ and $\mathcal{F}^{-1}$ denote the two-dimensional discrete Fourier transform and discrete inverse Fourier transform with respect to the (x, x') and (k, k') variables. The FFTs may be optimized by exploiting the hermicity of the density matrix.

Alternatively, we may calculate the von Neumann solution indirectly by solving the Schrödinger equation for several states and then using definition (2.7) to construct the density matrix. This simplifies a two-dimensional problem over N^2 grid-points to n independent one-dimensional problems over N grid-points. If the initial distribution is localized in phase space, n may be chosen to be appreciably smaller than N, saving not only memory but also contributing to a considerable reduction in computation time. Furthermore, this approach allows us to implement the solution using a parallel computer cluster. One way to implement such a scheme is to use states generated by taking thin slices of the initial distribution along the x-direction. Consider the WKB initial condition

$$(5.3) \qquad \psi(x, 0; \tilde{x}, \tilde{p}) = (\sigma_x \sqrt{2\pi})^{-1/4} \exp(-(x - \tilde{x})^2/4\sigma_x^2) \exp(i\tilde{p}x/\varepsilon),$$

which describes a wave packet with an $O(1)$ spread in position and $O(\varepsilon)$ spread in momentum. Let the weight distribution in the definition of the density matrix (2.7) be

$$(5.4) \qquad \tilde{f}(\tilde{x}, \tilde{p}) = \delta(\tilde{x} - x_0) \exp(-(\tilde{p} - p_0)^2/2s_\varepsilon^2 \sigma_p^2)/(s_\varepsilon^2 \sigma_p \sqrt{2\pi})$$

where the scaling factor $s_\varepsilon = 1/\sqrt{1 + (\varepsilon/2\sigma_x\sigma_p)^2}$. Then

$$\hat{\rho}(x, x', 0) = \iint_{-\infty}^{\infty} \tilde{f}(\tilde{x}, \tilde{p})\psi(x, 0; \tilde{x}, \tilde{p})\overline{\psi}(x', 0; \tilde{x}, \tilde{p}) \, d\tilde{x} \, d\tilde{p}$$

$$= \frac{1}{\sigma_x\sqrt{2\pi}} \exp\left(-\frac{(x - x_0)^2 + (x' - x_0)^2}{4\sigma_x^2} - \frac{(x - x')^2}{2\varepsilon^2 s_\varepsilon^{-2}\sigma_p^{-2}} - \frac{ip_0(x - x')}{\varepsilon}\right)$$

$$= \frac{1}{\sigma_x\sqrt{2\pi}} \exp\left(-\frac{(\frac{1}{2}(x + x') - x_0)^2}{2\sigma_x^2} - \frac{(x - x')^2}{2\varepsilon^2 \sigma_p^{-2}} - \frac{ip_0(x - x')}{\varepsilon}\right).$$

13

Using the Wigner transform (2.10), we have the equivalent Liouville initial distribution

$$(5.5) \qquad f(x, p, 0) = \frac{1}{2\pi\sigma_x\sigma_p} \exp\left(-\frac{(x - x_0)^2}{2\sigma_x^2} - \frac{(p - p_0)^2}{2\sigma_p^2}\right)$$

which is independent of ε.

To compare the convergence of the Schrödinger and von Neumann solution in the semiclassical limit, we use the L^1-error of the position probability density function (pdf),

$$\int_{-\infty}^{\infty} \left| \rho(x, t) - |\psi(x, t)|^2 \right| \, dx$$

with $\rho(x, t) = \int_{-\infty}^{\infty} f(x, p, t)\, dp$. We replace $|\psi(x, t)|^2$ with $\hat{\rho}(x, x, t)$ for the von Neumann solution. The semiclassical Liouville model should also predict the correct weak limit for multiphase solutions when interference in the Schrödinger and von Neumann solutions result in oscillations in the probability density distribution. To measure the weak convergence in the semiclassical limit, we determine the L^1-error in the cumulative distribution function (cdf), *i.e.*, the antiderivative of position density [11]

$$\int_{-\infty}^{\infty} \left| \int_{-\infty}^{x} \rho(s, t) - |\psi(s, t)|^2 \, ds \right| \, dx.$$

In each example we compare the exact or numerical semiclassical Liouville solution with numerical Schrödinger or von Neumann solutions for equivalent initial distributions and potentials. Since the interactions with the boundaries are not relevant to the study, a sufficiently large domain is chosen and simulation is stopped before the wave envelope reaches the boundaries.

5.1. Schrödinger $O(1)$ wave envelope with a step potential. Consider the step potential

$$(5.6) \qquad V(x) = \begin{cases} 0 & \text{if } x < 0, \\ \frac{1}{2} & \text{if } x > 0. \end{cases}$$

A particle impinging on this potential from the left is totally reflected when the incident velocity is less than 1.

We find the exact solution by the method of characteristics by tracing along the bicharacteristics backward in time to the initial conditions. Let $\Omega(t) = \{ (x, p) \mid x < 0 \text{ and } x - pt < 0, \text{ or } x > 0 \text{ and } x - pt > 0 \}$ be the region in phase space where the bicharacteristics have not crossed the quantum barrier at $x = 0$ within a time t. Then the exact solution

$$(5.7) \qquad f(x, p, t) = \begin{cases} f(x - pt, p, 0), & (x, p) \in \Omega(t) \\ T \cdot f\left(\frac{q}{p}x - qt, q, 0\right) + R \cdot f\left(-x + pt, -p, 0\right), & \text{otherwise} \end{cases}$$

where the incident velocity is given by $q = \sqrt{p^2 + 1}$ if $p > 0$ and $q = -\sqrt{p^2 - 1}$ if $p \leq 0$. From equations (4.3) and (4.7), the reflection coefficient is given by

$$R = \left| \frac{p - q}{p + q} \right|^2 = |p - q|^4.$$

14

Note that when $p \in [-1, 0]$, q is imaginary and $R = 1$ indicating total reflection.

Consider the WKB initial condition

$$\psi(x, 0) = A(x) e^{iS(x)/\varepsilon}$$

as a wavepacket generalization with the amplitude and phase functions given by

$$A(x) = (\pi\sigma^2)^{-1/4} e^{-(x-x_0)^2/\sigma^2}$$
$$S(x) = ax^2 + bx + c.$$

Since $S(x)$ is a quadratic function, we can calculate the Wigner transform of $\psi(x, 0)$ exactly to get

$$f(x, p, 0) = (\pi\varepsilon)^{-1} e^{(x-x_0)^2/\sigma^2} e^{-(2ax+b-p)^2/(\varepsilon/\sigma)^2}.$$

In the semiclassical limit ($\varepsilon \to 0$), we have

$$f(x, p, 0) = A^2(x)\delta(p - \nabla_x S(x))$$
(5.8)
$$= (\sigma\sqrt{\pi})^{-1} e^{-(x-x_0)^2/\sigma^2} \delta(p - (2ax + b)).$$

By taking $\sigma = O(1)$ in $A(x)$, we create a wave envelope that is independent of ε, allowing us to study the convergence of solutions as $\varepsilon \to 0$. When $a \neq 0$, the distribution of phases included in the Schrödinger solution is also $O(1)$.

Using the above semiclassical WKB initial conditions (5.8), we note that when $t = -1/2a$ the position density for the Liouville solution (5.7) exhibits a caustic with all bicharacteristics intersecting at either $x = b/2a$, or $x = -b/2a$ for reflected solutions. Because of the nonlinear change to the incident velocities, the transmitted bicharacteristics do not cross simultaneously resulting in a traveling front, the leading edge of which is unbounded.

Take $(x_0, p_0) = (-\frac{1}{2}, 1)$ and take $a = -\frac{1}{4}$, $b = p_0 - 2a = \frac{3}{2}$ and $\sigma = \frac{1}{10}$. Then we have the initial conditions

$$\psi(x, 0) = (10/\pi)^{1/4} e^{-200(x-x_0)^2} e^{i(ax^2 + (p_0 - 2ax_0)x)\varepsilon}$$

for the Schrödinger equation and

$$f(x, p, 0) = (10/\pi)^{1/2} e^{-100(x-x_0)^2} \delta(p - p_0 - 2a(x - x_0))$$

for the semiclassical Liouville equation. The numerical Schrödinger solution is solved using a Crank-Nicolson finite-difference method over the domain $[-1, 1]$ with mesh size $\Delta x = \Delta t = 10^{-6}$. The exact semiclassical Liouville solution is solved by tracking characteristics forward in time with values determined by the initial velocity given by $\nabla S = \frac{3}{4} - \frac{1}{2}x$. We compute the solution at time $t = 0.8$.

The position densities for several values of ε are shown in Fig. 5.1. The convergence results of the errors in the two solutions are listed in Table 5.1. Based on this study, we find that the l^1 convergence rate in ε of the pdf is about 0.6 and the l^1 convergence rate in ε of the cdf is about 1.1.

15

TABLE 5.1
Errors in solutions for different values of ε for Example 5.1.

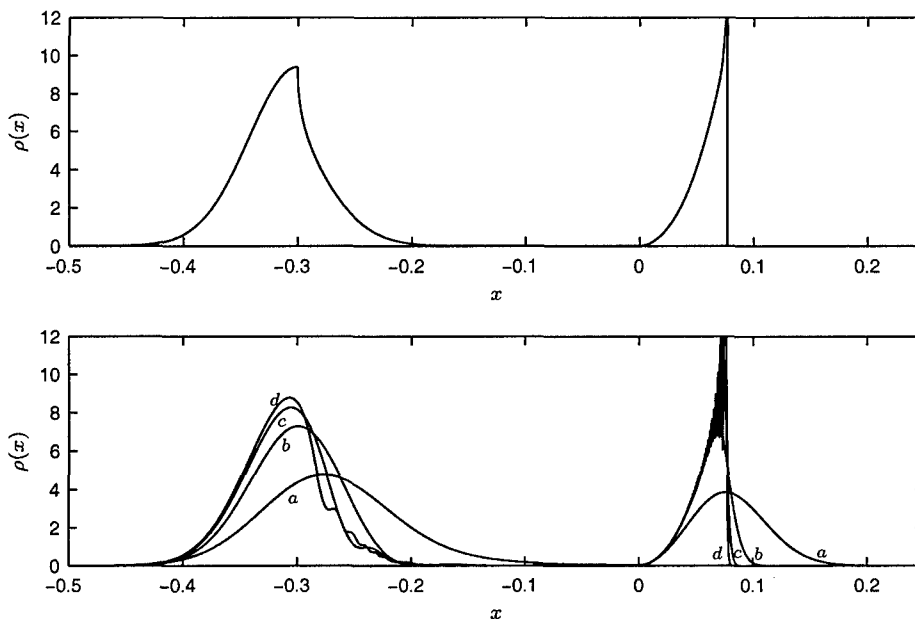| ε	200^{-1}	800^{-1}	3200^{-1}	12800^{-1}
l^1-error (pdf)	8.78×10^{-1}	3.37×10^{-1}	1.55×10^{-1}	8.61×10^{-2}
l^1-error (cdf)	5.15×10^{-2}	1.00×10^{-2}	2.28×10^{-3}	1.08×10^{-4}

FIG. 5.1. *Position densities for the semiclassical Liouville (top) and Schrödinger (bottom) solutions of Example 5.1. The Schrödinger solution shows $\varepsilon =$ (a) 200^{-1}, (b) 800^{-1}, (c) 3200^{-1} and (d) 12800^{-1}. The position density of Liouville solution exhibits a caustic near $x = 0.08$ and the peak is unbounded. For the Schrödinger solution the peak reaches a height of 19 for the $\varepsilon = 12800^{-1}$. The plots are truncated for clarity.*

5.2. Von Neumann solution with step potential. We now consider the solution to the von Neumann equation with the step potential given Example 5.1. To construct a von Neumann initial condition $\hat{\rho}(x, x', 0)$ which corresponds to a Liouville initial condition $f(x, p, 0)$, we may directly use the definition of the density matrix (2.7) for some weight function with the probability amplitudes $\psi(x, t)$ given by Gaussian ε-wavepackets

$$(5.9) \qquad \psi(x, 0) = (\pi\varepsilon)^{-1/4} e^{-(x-x_0)^2/2\varepsilon} e^{ip_0 x/\varepsilon}.$$

The Liouville initial condition may subsequently be calculated by a Wigner transform of the density matrix. Alternatively, we may construct the density matrix by using the inverse Wigner transform applied to the Liouville initial conditions $f(x, p, 0)$ to get

$$\hat{\rho}(x, x', 0) = \int_{-\infty}^{\infty} f(\tfrac{1}{2}(x + x'), p, 0) e^{ip(x-x')/\varepsilon} \, dp.$$

By taking the Liouville initial conditions to be the Gaussian

$$(5.10) \qquad f(x, p, 0) = \frac{1}{2\pi \sigma_x \sigma_p} \exp\left(\frac{-(x - x_0)^2}{2\sigma_x^2}\right) \exp\left(\frac{-(p - p_0)^2}{2\sigma_p^2}\right)$$

we may compute the von Neumann initial conditions exactly to get

$$(5.11) \quad \hat{\rho}(x, x', 0) = \frac{1}{\sigma_x \sqrt{2\pi}} \exp\left(-\frac{(\frac{1}{2}(x + x') - x_0)^2}{2\sigma_x^2} - \frac{(x - x')^2}{2\varepsilon^2 \sigma_p^{-2}} - \frac{i p_0 (x - x')}{\varepsilon}\right).$$

We chose $\sigma_x = \sigma_p = 0.05$, $x_0 = -0.5$ and $p_0 = 1.0$ and compared the solutions to the von Neumann and semiclassical Liouville equations at time $t = 1.0$. The von Neumann equation was solved using the psuedospectral method with Strang splitting over the domain $[-1, 1]$ with $\varepsilon = 64^{-1}$, 128^{-1}, 256^{-1} and 512^{-1}. The grid spacing was fixed at $\Delta x = 2048^{-1}$ with $\Delta t = (\Delta x)^2/\varepsilon$ to ensure consistency and stability. The exact solution to the semiclassical Liouville model is calculated using equation (5.7).

The position densities for the semiclassical Liouville solution and the von Neumann solution for several values of ε are shown in Fig. 5.2. The errors in the two solutions are listed in Table 5.2. Based on our study, we find the convergence rate of the l^1-error of the pdf is about 0.7 as $\varepsilon \to 0$ and the convergence of the l^1-error of the cdf is about 0.9 as $\varepsilon \to 0$.

TABLE 5.2
Errors in solutions of Example 5.2 for different values of ε .

ε	64^{-1}	128^{-1}	256^{-1}	512^{-1}
l^1-error (pdf)	6.03×10^{-1}	4.04×10^{-1}	2.50×10^{-1}	1.40×10^{-1}
l^1-error (cdf)	9.22×10^{-2}	4.83×10^{-2}	2.53×10^{-2}	1.32×10^{-2}

We may also consider the effect of incorporating barrier time delay in the approximation of the von Neumann equation for nonvanishing ε. As evident from the offset of the centers of the distributions on the left side of Fig. 5.2, one source of error is the time delay which vanishes in the semiclassical limit. The time delay may be considered as an $O(\varepsilon)$ correction and hence we may neglect it in the semiclassical limit. While the the addition of a delay time is numerically nontrivial, for the analytic solution (5.7) it is a straight-forward modification.

Typically, time delay is defined in terms of Wigner time delay, the delay to the group velocity of a wave packet resulting from reflection and transmission. As such it is meaningful when the wave packet has a well-defined peak. This is not generally the case, especially when the barrier is sufficiently wide. Considering the scattering relation (4.5), the reflection and transmission group delay times for unit mass are [26]

$$\tau_t = \frac{\varepsilon}{p} \frac{d}{dp} \arg t = \frac{\varepsilon}{p} \text{Im} \left(\frac{1}{t} \frac{dt}{dp}\right) \qquad \text{and} \qquad \tau_r = \frac{\varepsilon}{p} \frac{d}{dp} \arg r = \frac{\varepsilon}{p} \text{Im} \left(\frac{1}{r} \frac{dr}{dp}\right).$$

For the step potential (5.6), we have from equation (4.3) that the reflection time delay is

$$\tau_r = 2\varepsilon \text{Im} \left[(pq)^{-1}\right] = \frac{2\varepsilon}{p\sqrt{1 - p^2}}$$

when $p \in [-1, 0]$. There is no transmission or reflection delay time for $p \notin [-1, 0]$. To incorporate the time delay, we make the replacement

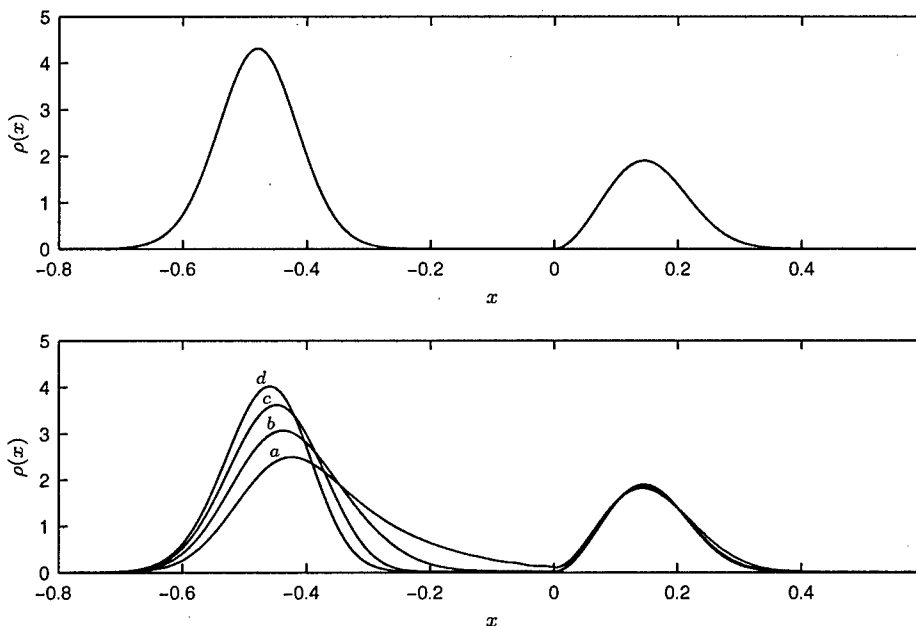$$f\left(-x + pt, -p, 0\right) \quad \to \quad f\left(-x + p(t + \tau_r), -p, 0\right)$$

17

FIG. 5.2. *Position densities for the semiclassical Liouville (top) and von Neumann (bottom) solutions of Example 5.2. The von Neumann plot shows ε equal to (a) 64^{-1}, (b) 128^{-1}, (c) 256^{-1} and (d) 512^{-1}.*

in the reflected term of the exact solution (5.7).

We compare the von Neumann solution with the Liouville solution with time delay correction. The l^1-errors are listed in Table 5.3. Based on this study, we find that the addition of delay time provides some improvement to the model. The convergence rate of the l^1-error of the pdf is about 1.3 and convergence rate of the l^1-error of the cdf is about 0.9 as $\varepsilon \to 0$.

TABLE 5.3
Errors in solutions of Example 5.2 with time delay correction.

ε	64^{-1}	128^{-1}	256^{-1}	512^{-1}
l^1-error (pdf)	3.67×10^{-1}	1.78×10^{-1}	7.05×10^{-2}	2.23×10^{-2}
l^1-error (cdf)	2.62×10^{-2}	1.65×10^{-2}	7.80×10^{-3}	3.90×10^{-3}

5.3. Von Neumann solution with two step potentials. We may consider more complicated geometries by considering multiple barriers. In this example we construct an $O(1)$-wide rectangular barrier by taking two step barriers sequentially. Consider

$$V(x) = \begin{cases} \frac{1}{2} & \text{if } x \in [0, \frac{1}{5}], \\ 0 & \text{otherwise.} \end{cases}$$

We take the initial conditions given in equations (5.10) and (5.11) with $\sigma_x = \sigma_p = 0.05$, $x_0 = -0.45$ and $p_0 = 1.1$. We compute over the domain $[-1.25, 1.25]$ and compare the

solutions at time $t = 1.2$. The von Neumann equation is solved using a pseudospectral method with Strang splitting as in Example 5.2. The semiclassical Liouville solution is solved using the numerical method proposed in §4 using N grid points in x and p and $1.5N$ steps in time. The results are shown in Fig. 5.3 with $\varepsilon = 0.002$. Even with a fairly coarse mesh, the numerical semiclassical solution agrees well with the von Neumann equation both in the strong limit away from the barrier and in the weak limit between the two step potentials. See Fig. 5.4.

We calculate convergence rate as Δx, Δp, $\Delta t \to 0$ of numerical scheme for the semiclassical Liouville equation by computing the l^1-error of the numerical solutions using a mesh with $N = 50$, 100, 200, and 400 grid points. For an "exact" solution, we use the numerical solution using $N = 3200$. The errors are listed in Table 5.4. Based on this study, we find the convergence rate of the numerical scheme using the l^1-norm is about 1.2.

TABLE 5.4
Errors in solutions of Example 5.3 for various mesh sizes Δx.

grid points	50	100	200	400
l^1-error	3.32×10^{-1}	1.15×10^{-1}	4.72×10^{-2}	2.56×10^{-2}

5.4. Resonant tunneling von Neumann solution. We present a final example to illustrate a specific physical model, the resonant tunneling diode (RTD) [19, 25, 30]. An RTD consists of thin layers (a few nanometers thick) of different semiconductors, such as gallium arsenide (GaAs) and aluminum gallium arsenide (AlGaAs), that are sandwiched together to form a double-barrier quantum well structure. For semiconductors the de Broglie wavelength is on the order of tens of nanometers, so the length of the entire RTD structure is on the length scale of a de Broglie wavelength. The region outside the barrier is doped to provide a sufficient number of free electrons. Unlike the transmission probabilities of the step potentials presented the previous examples, the transmission probability of an RTD is not a monotonic function of the incident particle energy. Rather, it is oscillatory and admits narrow peaks of total or almost total transmission well below the cutoff energy for classical transmission. By changing the bias voltage of an external electrostatic potential applied to the system, the resonance may be tuned to admit electrons of varying energies.

We shall assume that the electron trajectory is ballistic. In the quantum region, this simplification is appropriate since the electron mean free path is substantially larger than the barrier thickness. However, away from the barrier this simplification is physically unrealistic since the electron mean free path is small compared to the classical length scale for a dense medium. In this case, a relaxation term or collision operator should be added to the Liouville equation to capture the particle dynamics. Since we require that the Hamiltonian be only locally preserved, the model may be extended to a dissipative system, for which the Hamiltonian is continuous, without changing the approach discussed in §3 and §4. Hence, for the purpose of validation, the assumption is reasonable.

We construct a representative barrier

$$V(x) = \begin{cases} +\frac{1}{2}V_0 & x \in (-\infty, -a-b] \\ -\frac{1}{2}V_0 x/(a+b) + V_b & x \in (-a-b, -a] \cup (a, a+b] \\ -\frac{1}{2}V_0 x/(a+b) & x \in [-a, a+b] \\ -\frac{1}{2}V_0 & x \in (a+b, \infty) \end{cases}$$
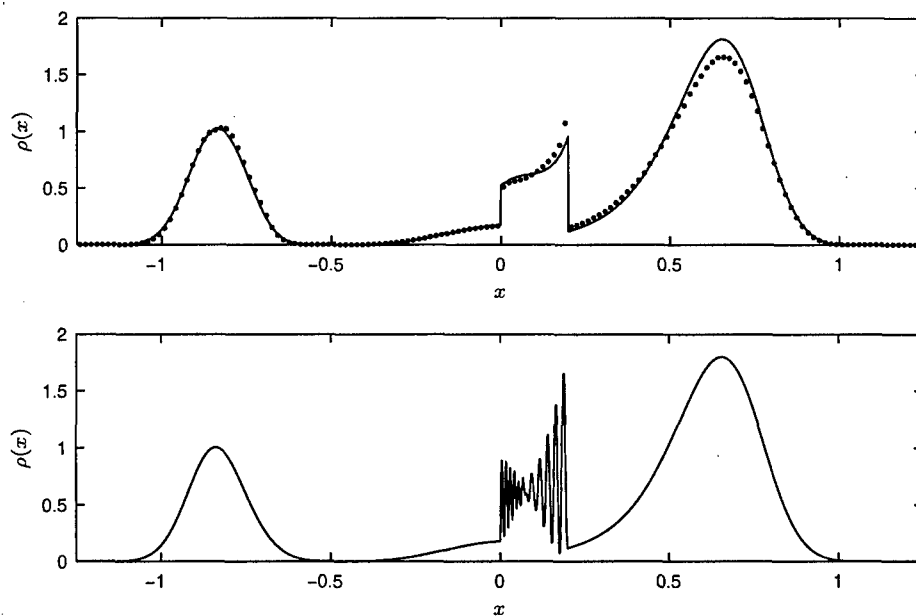
19

FIG. 5.3. *Position densities for the numerical semiclassical Liouville (top) and von Neumann (bottom) solutions of Example 5.3. The • in the Liouville plot shows the numerical solution for with 150 grid points over the domain* [−1.25, 1.25]. *The solid line shows the numerical solution for 3200 grid points. The von Neumann solution is for* $\varepsilon = 0.002$.
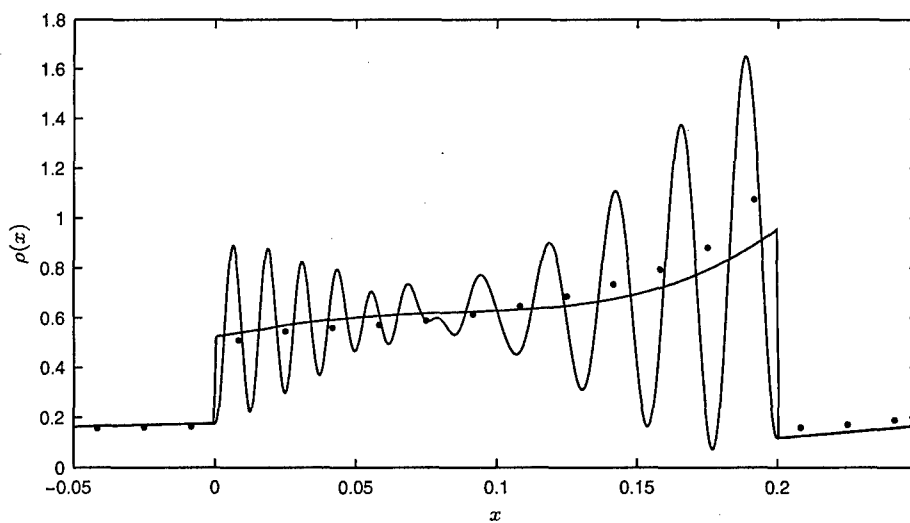

FIG. 5.4. *Detail of Fig. 5.3 showing position densities for the numerical semiclassical Liouville and von Neumann solutions. The • shows the numerical solution for with 150 grid points over the domain* [−1.25, 1.25]. *The solid line shows the "exact" Liouville solution and the von Neumann solution using* $\varepsilon = 0.002$.
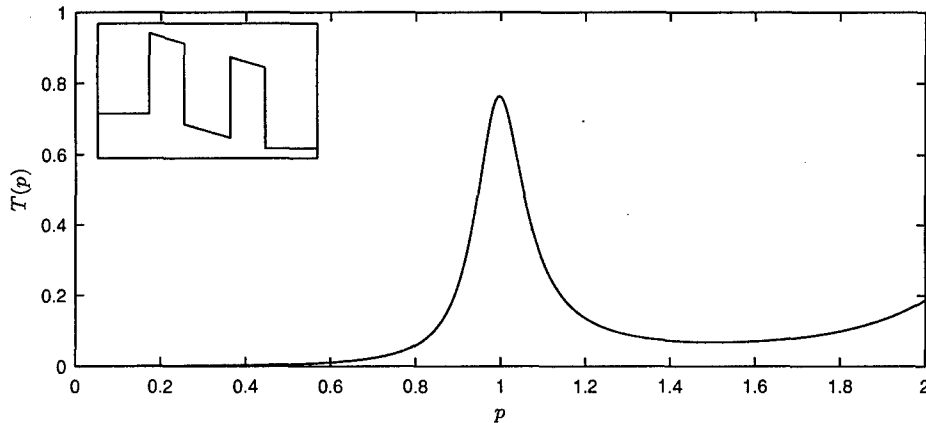
20

FIG. 5.5. *Transmission probability as function of the momentum p for the RTD barrier—shown in the inset—presented in Example 5.4.*

where the external potential bias $V_0 = 0.48$, the thickness of each barrier $b = 0.9\varepsilon$, the thickness of the well separating the barriers $2a = 1.2\varepsilon$, and the height of each barrier $V_b = 2.25$. See Fig. 5.5. We take Gaussian initial distributions (5.10) and (5.11) with $\sigma_x = 0.05$, $\sigma_p = 0.15$, $x_0 = -1$ and $p_0 = 1$. The solutions are computed over the domain $[-4, 4]$ and compared at time $t = 2.5$.

The von Neumann equation is solved indirectly using the WKB initial conditions (5.3) with weight distribution (5.4). We use a Crank-Nicolson finite-difference method to solve the Schrödinger equations. To ensure that the weight function is sufficiently resolved, we take $N = (5\varepsilon)^{-1}$ Schrödinger solutions with initial values equally spaced over $8\sigma_p$ about p_0.

The semiclassical Liouville solution is solved using the numerical method proposed in §4 using an N grid points over $[-4, 4]$ in x, $2N$ grid points over $[-3, 3]$ in p and $3N$ steps in time. The exact solution is computed using equation (5.7) with transmission and reflection probabilities calculated using the transfer matrix method. In computing the transfer matrix for both the numerical and exact solutions, the quantum barrier is discretized using 2000 grid point over the length 6ε for an arbitrary ε. The results are shown in Fig. 5.6 and Table 5.5. We calculate an l^1-convergence rate of 1.7 in $\Delta x, \Delta p, \Delta t$.

TABLE 5.5
Errors in solutions of Example 5.4 for various mesh sizes Δx.

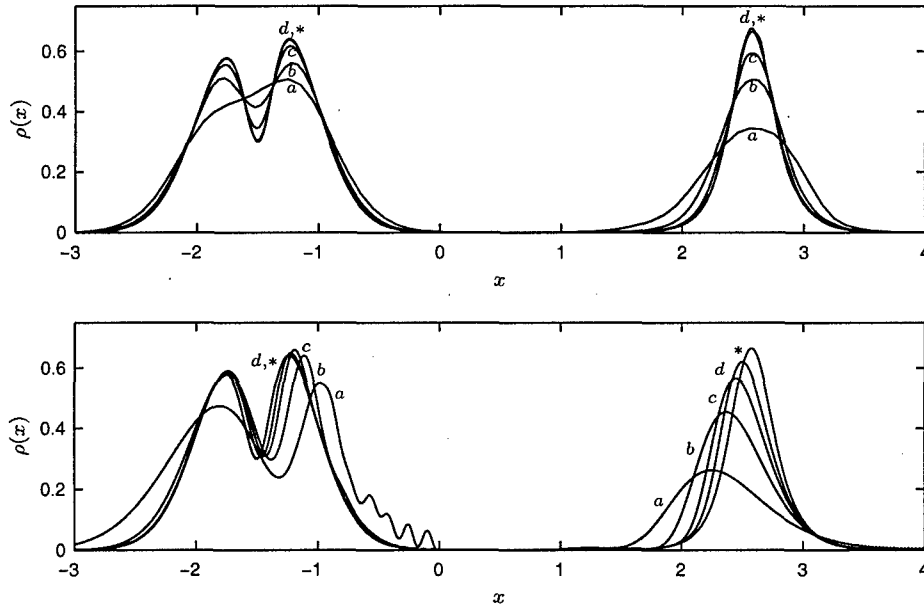| grid points	80	160	320	640
l^1-error	3.01×10^{-1}	1.37×10^{-1}	4.43×10^{-2}	8.90×10^{-3}

REFERENCES

21

FIG. 5.6. *Position densities for the numerical semiclassical Liouville (top) and von Neumann (bottom) solutions of Example 5.4. The Liouville solution shows the numerical solution for (a) 80, (b) 160,(c) 320 and (d) 640 grid points. The von Neumann solution is plotted for $\varepsilon = $ (a) 50^{-1}, (b) 100^{-1}, (c) 200^{-1} and (d) 400^{-1}. The exact solution (*) is also plotted in each case.*

[1] Y. ANDO AND T. ITOH, *Calculation of transmission tunneling current across arbitrary potential barriers*, J. Appl. Phys., 61 (1987), pp. 1497–1502.

[2] A. ARNOLD, *Mathematical concepts of open quantum boundary conditions*, Transport Theor. Stat., 30 (2001), pp. 561–584.

[3] G. BAL, J. B. KELLER, G. PAPANICOLAOU, AND L. RYZHIK, *Transport theory for acoustic waves with reflection and transmission at interfaces*, Wave Motion, 30 (1999), pp. 303–327.

[4] W. BAO, S. JIN, AND P. A. MARKOWICH, *On time-splitting spectral approximations for the Schrödinger equation in the semiclassical regime*, J. Comput. Phys., 175 (2002), pp. 487–524.

[5] ———, *Numerical study of time-splitting spectral discretizations of nonlinear Schrödinger equations in the semi-clasical regimes*, SIAM J. Sci. Comp., 25 (2003), pp. 27–64.

[6] N. BEN ABDALLAH, *A hybrid kinetic-quantum model for stationary electron transport*, J. Stat. Phys., 90 (1998), pp. 627–662.

[7] N. BEN ABDALLAH, P. DEGOND, AND I. M. GAMBA, *Coupling one-dimensional time-dependent classical and quantum transport models*, J. Math. Phys., 43 (2002), pp. 1–24.

[8] N. BEN ABDALLAH AND S. TANG, *On hybrid quantum-classical transport models*, Math. Methods Appl. Sci., 27 (2004), pp. 643–667.

[9] A. O. BOLIVAR, *Quantum-classical Correspondence*, The Frontiers Collection, Springer, New York, 2004.

[10] P. GÉRARD, P. A. MARKOWICH, N. J. MAUSER, AND F. POUPAUD, *Homogenization limits and Wigner transforms*, Comm. Pure Appl. Math., 50 (1997), pp. 323–379.

[11] L. GOSSE AND N. J. MAUSER, *Multiphase semiclassical approximation of an electron in a one-dimensional crystalline lattice. III. From ab initio models to WKB for Schrödinger-Poisson*, J. Comput. Phys., 211 (2006), pp. 326–346.

[12] P. GROSSEL AND J. M. VIGOUREUX, *Nonlocal approach to scattering in a one-dimensional problem*, Phys. Rev. A, 50 (1994), pp. 3627–3637.

[13] B. HELLSING AND H. METIU, *An efficient method for solving the quantum Liouville equation: applications to electronic absorption spectroscopy*, Chem. Phys. Lett., 127 (1986), pp. 45–49.

[14] S. JIN AND X. LI, *Multi-phase computations of the semiclassical limit of the Schrödinger equation and related problems: Whitham vs. Wigner*, Phys. D, 182 (2003), pp. 46–85.

[15] S. JIN AND X. WEN, *A Hamiltonian-preserving scheme for the Liouville equation of geometrical optics with transmissions and reflections*, SIAM J. Numer. Anal. submitted.

[16] ——, *Hamiltonian-preserving schemes for the Liouville equation of geometrical optics with discontinuous local wave speeds*, J. Comp. Phys., xxx (2005), pp. xxx–xxx.

[17] ——, *Hamiltonian-preserving schemes for the Liouville equation with discontinuous potentials*, Commun. Math. Sci., 3 (2005), pp. 285–315.

[18] B. JONSSON AND S. T. ENG, *Solving the Schrödinger equation in arbitrary quantum-well potential profiles using the transfer-matrix method*, IEEE J. Quantum Elect., 726 (1990), pp. 2025–2035.

[19] N. C. KLUKSDAHL, A. M. KRIMAN, D. K. FERRY, AND C. A. RINGHOFER, *Self-consistent study of the resonant runneling fiode*, Phys. Rev. B., 39 (1989), pp. 7720–7735.

[20] C. S. LENT AND D. J. KIRKNER, *The quantum transmitting boundary method*, J. Appl. Phys., 67 (1990), pp. 6353–6359.

[21] R. J. LEVEQUE, *Finite Volume Methods for Hyperbolic Problems*, Cambridge Texts in Applied Mathematics, Cambridge University Press, Cambridge, 2002.

[22] P.-L. LIONS AND T. PAUL, *Sur les mesures de Wigner*, Rev. Mat. Iberoamericana, 9 (1993), pp. 553–618.

[23] V. A. MANDELSTAHM AND H. S. TAYLOR, *Spectral projection approach to the quantum scattering calculations*, J. Chem. Phys., 102 (1995), pp. 7390–7398.

[24] P. A. MARKOWICH, P. PIETRA, AND C. POHL, *Numerical approximation of quadratic observables of Schrödinger-type equations in the semi-classical limit*, Numer. Math., 81 (1999), pp. 595–630.

[25] P. A. MARKOWICH, C. A. RINGHOFER, AND C. SCHMEISER, *Semiconductor Equations*, Springer-Verlag, Vienna, 1990.

[26] A. MESSIAH, *Quantum Mechanics. Vol. I*, Translated from the French by G. M. Temmer, North-Holland Publishing Co., Amsterdam, 1961.

[27] L. MILLER, *Refraction of high-frequency waves density by sharp interfaces and semiclassical measures at the boundary*, J. Math. Pures Appl. (9), 79 (2000), pp. 227–269.

[28] L. RYZHIK, G. C. PAPANICOLAOU, AND J. B. KELLER, *Transport equations for waves in a half space*, Comm. Partial Differential Equations, 22 (1997), pp. 1869–1910.

[29] C. SPARBER, P. A. MARKOWICH, AND N. J. MAUSER, *Wigner functions versus WKB-methods in multivalued geometrical optics*, Asymptot. Anal., 33 (2003), pp. 153–187.

[30] J. P. SUN, G. I. HADDAD, P. MAZUMDER, AND J. N. SCHULMAN, *Resonant tunneling diodes: Modes and properties*, P. IEEE, 86 (1998), pp. 641–661.

[31] E. WIGNER, *On the quantum correction for thermodynamic equilibrium*, Phys. Rev., 40 (1932), pp. 749–759.